

# A highly selective dual-signal response ratiometric fluorescence sensing strategy for malachite green in fish based on carbon dots/copper nanoclusters nanocomposite

Jun-Qiu Zhang<sup>a</sup>, Xiao-Fang Shen<sup>a,\*</sup>, Jun Liu<sup>b,\*</sup>

<sup>a</sup> School of Food Science and Technology, Jiangnan University, Wuxi 214122, China

<sup>b</sup> Technology Center of Chengdu Customs, Chengdu 610041, China

## ARTICLE INFO

### Keywords:

Carbon dots  
Copper nanoclusters  
Ratiometric fluorescence  
Malachite green

## ABSTRACT

Malachite green (MG), a widely used antiparasitic agent, poses health risks to human due to its genotoxic and carcinogenic properties. Herein, a stable dual-emission fluoroprobe of carbon dots/copper nanoclusters is prepared for highly selective detection of MG based on the inner filter effect. This probe exhibits characteristic emission bands at 435 and 625 nm when excited at 376 nm. After adding MG, the both emission signals were significantly quenched, and the ratio of fluorescence intensity ( $F_{435}/F_{625}$ ) was linearly related to the concentration of MG in the range of 0.05–40  $\mu\text{mol L}^{-1}$  with a limit of detection of 18.2  $\text{nmol L}^{-1}$ . Meanwhile, the two signals exhibit linear relationships with the concentration of MG, respectively, and the corresponding detection results were consistent. The fluoroprobe was successfully used for the detection of MG in fish samples with the recoveries ranging from 96.0% to 103.8% and a relative standard deviation of <3.3%.

## 1. Introduction

Malachite green (MG) is a synthetic triphenylmethane compound that is extensively employed as a bactericide, parasiticide, and preservative in aquaculture and fisheries, primarily due to its robust antibacterial properties (Culp & Beland, 1996). Furthermore, MG is highly soluble in water, ethanol, and methanol, giving its solutions a distinctive blue-green hue. This versatility has led to its extensive use as a dye in industries of textiles, leather, paper, food and cosmetics (Samiey & Toosi, 2010). MG is easily absorbed by fish, while tending to accumulate in aquatic products and persist in the environment for a prolonged period. Through the food chain, MG harms the human health with a series of side effects such as carcinogenesis, teratogenicity and mutation induction (Culp et al., 1999; Srivastava, Sinha, & Roy, 2004; Wan, Weng, Liang, Lu, & He, 2011). Many countries and regions have enacted laws and regulations to restrict the use of MG, including the United State, China and the European Union. Nonetheless, MG is still illegally used in aquaculture due to its efficiency, availability, and lack of substitutes (Gao et al., 2019; Khan & Lively, 2020). It is important to develop an analytical method for detecting MG residues in aquatic products.

Nowadays, food safety is receiving increasing attention. Researchers

have developed various detection methods according to the different characteristics of the targets, such as high-performance liquid chromatography (HPLC) (Andersen et al., 2009), liquid chromatography-mass spectrometry (Li et al., 2020), thin-layer chromatography (Kraai, Rorer, & Wang, 2019), electrochemical analysis (He et al., 2023; Jiang et al., 2024; Luo & Li, 2022; Magesa et al., 2019; Sacara, Cristea, & Muresan, 2017; Sanjay et al., 2022), spectrophotometry (Yu et al., 2015), enzyme-linked immunosorbent assay (Shen et al., 2011; Wang et al., 2016), and surface-enhanced Raman spectroscopy (Chen, Huang, Miao, Fan, & Lai, 2023), and fluorescence sensing (Kong, Hou, Gong, Zhao, & Han, 2022; Yue et al., 2023). Among these methods, fluorescence sensing has attracted the attention of researchers due to its fast response, high sensitivity, simple operation, and cost-effectiveness. Li et al. (Z. Y. Li, Shen, Gu, & Chattha, 2022) developed a polyethylene pyrrolidone-gold-copper nanoclusters-based fluorescent sensor for the detection of MG in aquatic product, with excitation/emission peaks at 390/605 nm. Cheng et al. (Cheng, Wang, Yan, Xiao, & Zhang, 2022) prepared nitrogen-doped carbon dots (N-CDs) with green fluorescence (emission wavelength of 535 nm) using carmine base and disodium ethylenediaminetetraacetic acid as raw materials, which exhibit a rapid and sensitive response to MG. However, the traditional fluorescence methods typically rely on a single fluorescence signal for measurement,

\* Corresponding authors.

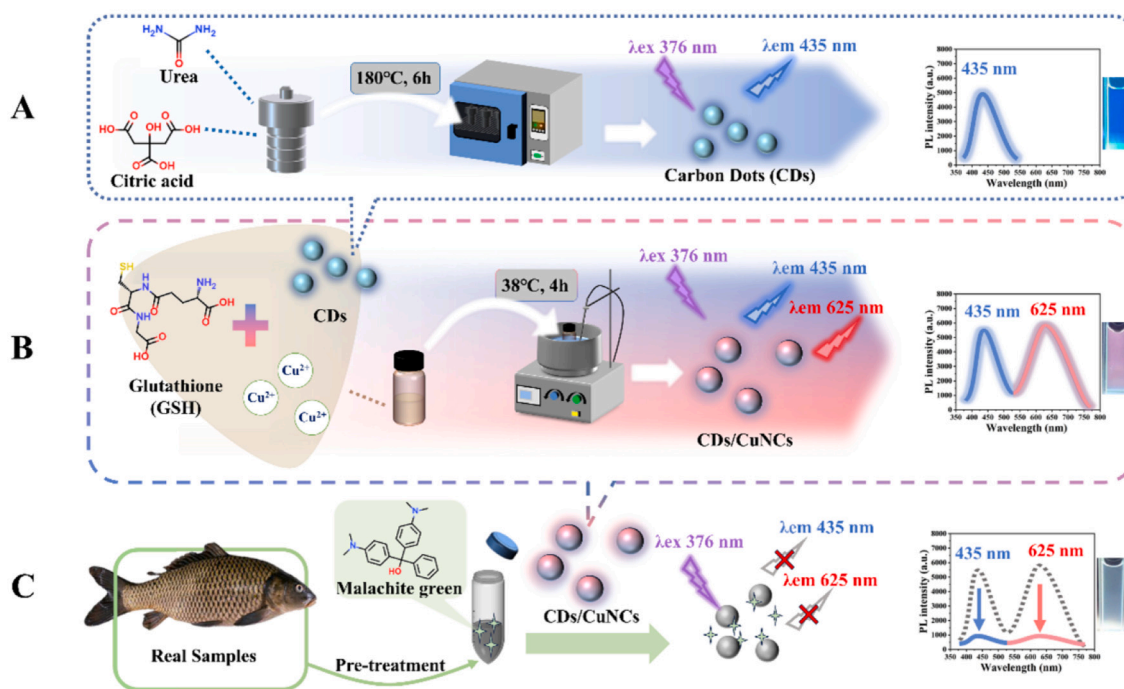
E-mail addresses: [xfshen@jiangnan.edu.cn](mailto:xfshen@jiangnan.edu.cn) (X.-F. Shen), [47575290@qq.com](mailto:47575290@qq.com) (J. Liu).

<https://doi.org/10.1016/j.foodchem.2024.139543>

Received 16 March 2024; Received in revised form 23 April 2024; Accepted 1 May 2024

Available online 8 May 2024

0308-8146/© 2024 Elsevier Ltd. All rights are reserved, including those for text and data mining, AI training, and similar technologies.



**Scheme 1.** (A). Schematic illustration of the process to prepare CDs; (B) the process to prepare CDs/CuNCs; (C) the detection of MG in fish by CDs/CuNCs.

which is easily affected by instrument noise, light source intensity, probe concentration, and surrounding environment (Qiu et al., 2022; Qu, Chen, Zheng, Cao, & Liu, 2013; Yan et al., 2015).

Ratiometric fluorescence sensor overcomes the fore-mentioned shortcomings by employing two emission wavelengths as detection and reference signals, enhancing the signal-to-noise ratio through built-in background interference correction, and ultimately improving detection reproducibility (Pei, Pan, Zhang, & Lv, 2021). Zhou et al. (Zhou, Zhou, & Chu, 2022) established a ratiometric fluorescence sensor for MG by immobilizing acridin-9-amine and rhodamine B (emitting blue and red fluorescence at 432 and 604 nm as a reference and detection signal, respectively) on UiO-66-(COOH)<sub>2</sub>, exhibiting stability performances with an RSD of <4.8%. Nevertheless, during the analysis of real samples, the presence of coexisting substances may produce false positives and lead to error analysis result. Given this challenge, further improvements in the recognition capabilities and the selectivity of the ratiometric fluorescence method become urgent.

In this study, we synthesized a dual-signal fluorescence nanocomposite, composed of CDs and CuNCs, and it was specifically designed to exhibit fluorescence at wavelengths that correspond to the two typical absorption peaks of MG. Based on the inner filter effect (IFE), we employed a dual-signal responsive ratiometric fluorescence detection strategy, establishing a highly selective and sensitive detection method for MG, which was applied to determine MG in fish samples (Scheme 1). The ratiometric signals of the probe exhibited self-correction properties, eliminating interference from the detection environment. Furthermore, its dual-signal response was capable of identifying false positive errors. This method can be applied to food safety food safety analysis, environmental monitoring and bioanalysis.

## 2. Experimental

### 2.1. Chemicals and instrumentation

Copper sulfate (CuSO<sub>4</sub>·5H<sub>2</sub>O, >99%) and sodium hydroxide (NaOH, >96%) were purchased from Beijing Chemical Co. (Beijing, China). Citric acid was purchased from J&K Scientific (Beijing, China). Metal salts (K<sup>+</sup>, Na<sup>+</sup>, Mg<sup>2+</sup>, Ca<sup>2+</sup>, Ba<sup>2+</sup>, Co<sup>2+</sup>, Hg<sup>2+</sup>, Cd<sup>2+</sup>, Cr<sup>2+</sup>, Pb<sup>2+</sup>, Zn<sup>2+</sup>,

Al<sup>3+</sup>, Fe<sup>3+</sup>), Dyes (Methylene blue (MB), methyl violet (MV), alizarin red (AR), crystal violet (CV), congo red (CR)), sodium nitrite was obtained from Aladdin (Shanghai, China). Antibiotic (tetracycline, chloramphenicol, sulfadiazine) were obtained from Solarbio Science & Technology Co., Ltd. (Beijing, China), suger (glucose, levulose, Cane sugar) was obtained from Sinopharm Chemical Reagent Co., Ltd. (Shanghai, China). Britton-Robison (BR) buffer was used in this study and consisted of 0.2 mol L<sup>-1</sup> sodium hydroxide solution in 0.04 mol L<sup>-1</sup> triacid (phosphoric acid, boric acid, acetic acid). BR buffer solutions with different pH values were configured using a pH meter. All aqueous solutions were prepared using deionized water obtained from a Millipore water purification system (≥18.2 MΩ cm, Milli-Q, Millipore).

The morphological detection results of CuNCs obtained by the transmission electron microscopy (TEM) with FEI Tecnai G2 F20 (FEI, Hillsboro, OR, U.S.). The ultraviolet-visible (UV-vis) absorption spectra and fluorescence spectra were measured on a TU-1901 Ultraviolet-visible spectrophotometer (Purkay, Beijing, China) and F-7000 fluorescence spectrometer (Hitachi, Ltd., Marunouchi, Tokyo, Japan), respectively. The Fourier transform infrared spectroscopy (FT-IR) and X-ray photoelectron spectroscopy (XPS) were recorded on a VERTEX 70 Fourier transform infrared spectrometer (Bruker, Ettlingen, Germany) and Escalab 250Xi X-ray photoelectron spectrometer (Thermo Fisher, Waltham, MA, U.S.), respectively.

### 2.2. Synthesis of CDs

The blue-emitting CDs was prepared via a one-step hydrothermal method with some modifications (Zhu et al., 2013). 0.30 g of citric acid and 1.5 g urea were dissolved in 30 mL of ultrapure water and stirred thoroughly. The solution was then transferred to a stainless-steel high-pressure reactor lined with polytetrafluoroethylene (PTFE) and heated at 180 °C in an oven for 6 h. After the completion of the reaction, the solution was naturally cooled to room temperature and subjected to filtration and centrifugation (5000 rpm, 5 min) to remove insoluble large particle impurities. The resulting mixture was further purified by dialysis (5000 Da) for 24 h to remove unreacted precursors, yielding a purified solution of carbon dots (CDs). The purified CDs solution was stored at 4 °C in a refrigerator for subsequent experiments. A portion of

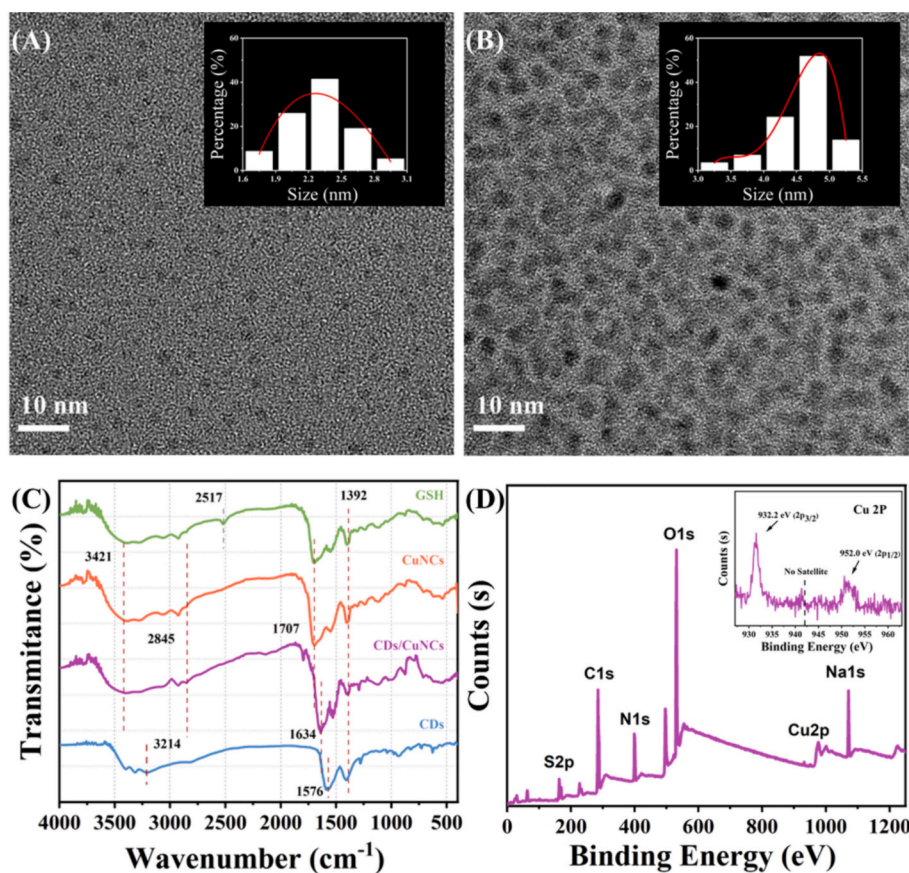


**Fig. 1.** (A, B) TEM of CDs and CDs/CuNCs, inset: the distribution of particle sizes; (C) FT-IR spectra of GSH, CuNCs, CDs and CDs/CuNCs; (D) XPS survey spectra of CDs/CuNCs, inset: XPS narrow scan spectra of Cu.

the sample was freeze-dried to obtain a solid powder sample for characterization.

### 2.3. Synthesis of CDs/CuNCs

The CDs/CuNCs nanocomposite was synthesized on the basis of a previous study (Li et al., 2020). GSH ( $12.5 \text{ mg mL}^{-1}$ , 5 mL),  $\text{CuSO}_4 \cdot 5\text{H}_2\text{O}$  ( $6 \text{ mg mL}^{-1}$ , 2 mL), and the purified CDs solution ( $12 \text{ mg mL}^{-1}$ , 2 mL) were mixed and diluted with ultrapure water to a 20 mL solution, and white emulsion was obtained after vortex. Subsequently, add  $1.0 \text{ mol L}^{-1}$  NaOH solution dropwise until the white emulsion gradually becomes clear, corresponding to a pH value of 4.0–5.0. Transfer the solution to a brown bottle and heat it in a water bath at  $38 \text{ }^\circ\text{C}$  for 4 h, resulting in a slightly yellowish clear solution. Purify the solution using dialysis in the dark for 24 h to remove the precursor. Store the purified CDs/CuNCs sample in a refrigerator at  $4 \text{ }^\circ\text{C}$  for subsequent use.

### 2.4. Detection of MG detection by CDs/CuNCs

Prepare a standard solution of MG or actual sample solution using ultrapure water. Dilute the prepared CuNCs solution three-fold with BR buffer (pH = 7.0) as a control group. Add 1 mL of the ultrapure water-prepared MG solution ( $10 \text{ nmol L}^{-1}$ ) to 1 mL of the CDs/CuNCs solution ( $1.5 \text{ mg mL}^{-1}$ ), incubate for 3 min, mix with 1 mL of the standard MG solution or sample extract of different concentrations, and incubate for 10 min. Measure the fluorescence intensity of the solution under excitation at 376 nm, the fluorescence signal of the nanocomposites is quenched at 435 nm and 625 nm. The quantitative detection of MG is achieved based on the fluorescence quenching degree of CDs/CuNCs. All experiments were carried out at room temperature and repeated three

times.

To establish correlation curves of fluorescence intensity of CDs/CuNCs and the concentration of MG, we prepared a series of MG solutions with different concentrations and obtained fluorescence spectra through experiments using the aforementioned detection method. The data was processed using Origin software to obtain the correlation curves between  $[(F_0 - F)/F_0]$  and MG concentration (where  $F_0$  represents the fluorescence intensity of the blank solution, and  $F$  represents the fluorescence intensity after adding MG). Since this fluorescent probe has two fluorescence emission peaks at 435 nm and 625 nm, two correlation curves were obtained based on the above steps. Additionally, we also established the correlation curves between the intensity ratio of these two fluorescence signals and the concentration of MG solution.

To evaluate the selectivity of the detection system, we added common coexisting substances at a concentration of  $0.3 \text{ mmol L}^{-1}$  to the CDs/CuNCs fluorescence system (replacing MG in the aforementioned detection method), including antibiotics (tetracycline, chloramphenicol, and sulfamethazine), amino acids (L-cysteine, glutathione, phenylalanine, and tyrosine), organic dyes (methylene blue, methyl violet, alizarin red, crystal violet, and methyl red), sugar additives (glucose, fructose, and sucrose), heavy metal ions ( $\text{Hg}^{2+}$ ,  $\text{Cd}^{2+}$ ,  $\text{Cr}^{3+}$ ,  $\text{Cu}^{2+}$ , and  $\text{Pb}^{2+}$ ), common anions and cations ( $\text{K}^+$ ,  $\text{Na}^+$ ,  $\text{Mg}^{2+}$ ,  $\text{Ca}^{2+}$ ,  $\text{Ba}^{2+}$ ,  $\text{Co}^{2+}$ ,  $\text{Fe}^{3+}$ ,  $\text{Zn}^{2+}$ ,  $\text{Al}^{3+}$ ,  $\text{NO}_3^-$ ,  $\text{Cl}^-$ , and  $\text{SO}_4^{2-}$ ).

To assess the anti-interference ability of the detection system, we added the aforementioned substances at a concentration of  $0.3 \text{ mmol L}^{-1}$  to the CDs/CuNCs fluorescence system in the presence of MG (where the concentration of  $\text{Fe}^{3+}$ ,  $\text{Zn}^{2+}$ ,  $\text{Pb}^{2+}$ , and  $\text{Al}^{3+}$  was adjusted to  $0.09 \text{ mmol L}^{-1}$ ).

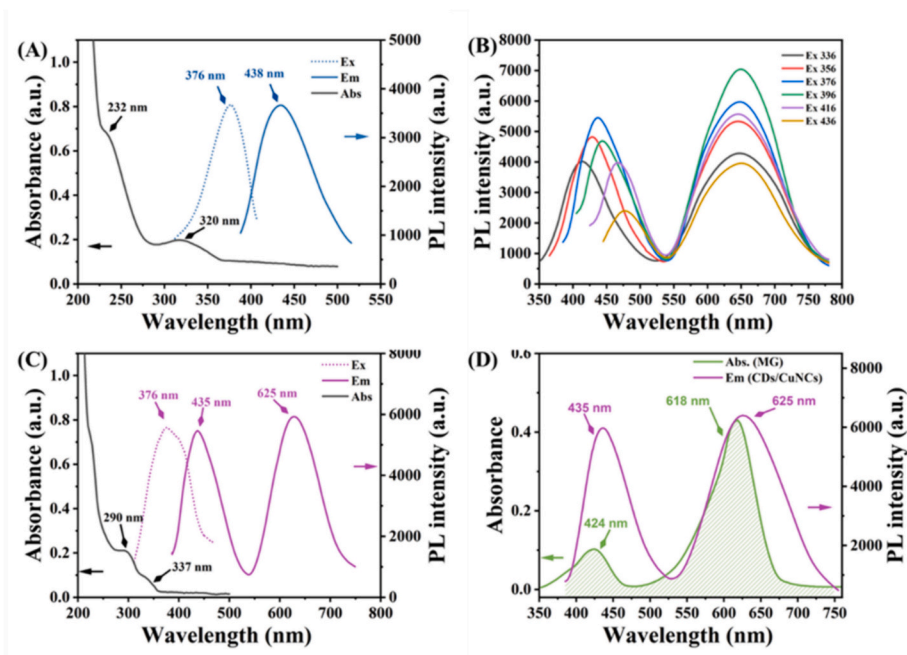


**Fig. 2.** (A) UV-vis absorption spectra and fluorescence spectra of  $0.5 \text{ mg mL}^{-1}$  BR buffer (pH = 7) of CDs; (B) Excitation wavelength dependence of CDs/CuNCs; (C) UV-vis absorption spectra and fluorescence spectra of  $1.5 \text{ mg mL}^{-1}$  BR buffer (pH = 7) CDs/CuNCs; (D) UV-vis absorption spectra of MG and fluorescence emission spectra of CDs/CuNCs (the shaded part represents the overlap of the two spectra).

### 2.5. Pretreatment of the fish sample and detection

The fish (silver carp and common carp) used as samples were freshly slaughtered and purchased from local supermarkets in Wuxi, China. The fish tissue processing method mainly followed the procedure outlined in reference (Luo et al., 2019). Accurately weigh 1 g of fish dorsal tissue, completely crush it, and dissolve it in 5 mL of acetonitrile. After sonication and centrifugation (at 12,000 rpm) for 5 min, the supernatant obtained is considered as the sample solution for detection.

To detect MG in the fish samples, different concentrations of MG (0, 1.0, 5.0, 10.0,  $15.0 \mu\text{mol L}^{-1}$ ) were injected into solutions containing CDs/CuNCs and the sample supernatant. The fluorescence intensity at 435 nm and 625 nm were then recorded. Recovery rate and relative standard deviation (RSD) were calculated. Please note that during the experimental procedure, it is important to follow safety protocols and strictly control experimental conditions to ensure accuracy and repeatability of the results.

### 2.6. Detection of MG detection by HPLC method

According to the national standards of the People's Republic of China GB/T 20361–2006, the HPLC method was employed. The measurement conditions are shown in Table S4.

## 3. Results and discussion

### 3.1. Design strategy and synthesis of CDs/CuNCs for MG

Based on MG's two absorption peaks within the range of 300–700 nm (424 nm and 618 nm) (Cheng et al., 2022), we designed a dual-signal recognition fluoroprobe to detect MG by IFE. To construct the nano-composite fluoroprobe, CDs with tunable fluorescence emission (Esmail & Jabbar, 2023) and CuNCs with a large Stokes shift (Sharma et al., 2023) were selected as components. First, we prepared CDs using the hydrothermal method with citric acid and urea as the precursors, by optimizing the reaction time and temperature. The CDs emit at 435 nm under 376 nm excitation, which matches the absorption peak of MG at

424 nm. Then, to match the absorption peak of MG at 618 nm simultaneously, we synthesized glutathione-modified CuNCs and combined it with the CDs. The synthesis process was optimized by adjusting the material ratio, reaction time, and temperature (as shown in Fig. S1), and the corresponding information is provided in the Supplementary Material.

### 3.2. Characterization of the CDs/CuNCs

We analyzed the morphology and the size of CDs and CDs/CuNCs by transmission electron microscope (TEM). Fig. 1(A, B) demonstrates that both CDs and CDs/CuNCs exhibit discrete microsphere structures. The particle size distribution for CDs ranges from 1.72 to 3.08 nm, with an average diameter of 2.32 nm ( $n = 50$ ), while for CDs/CuNCs, the distribution ranges from 3.10 to 5.24 nm, with an average diameter of 4.59 nm ( $n = 50$ ). In Fig. 1(C), GSH, CuNCs, CDs and CDs/CuNCs were characterized by FT-IR spectra. The broad and strong bands between 3420 and  $2845 \text{ cm}^{-1}$  are due to the O-H/N-H (Simoes, Leitao, & da Silva, 2016), and two characteristic absorption bands located at 1707 and  $1392 \text{ cm}^{-1}$  are assigned to the stretching vibration modes of C=O and C–N, respectively. The results indicated that there is carboxyl (–COOH) and amino (–NH<sub>2</sub>) groups on the surface of CuNCs similar to those found on GSH (Z. L. Li et al., 2021; Y. Y. Zhang et al., 2021). Besides, the peak at  $2517 \text{ cm}^{-1}$  is due to the stretching vibration of sulfhydryl group (S–H), which is present in the FT-IR spectrum of GSH, but disappeared in the CuNCs, which indicated the formation of the covalent bonds between GSH and CuNCs (Cu–S) (Bai et al., 2020). In the FT-IR spectrum of CDs, the band at  $3214 \text{ cm}^{-1}$ ,  $1576 \text{ cm}^{-1}$  and  $1392 \text{ cm}^{-1}$  correspond to O-H/N-H, C=O, N–H vibration, respectively, indicating the presence of –COOH and –NH<sub>2</sub> on the surface of CDs. The presence of –CONH group vibration peaks at approximately  $1634 \text{ cm}^{-1}$  suggests that the carboxyl and amino groups on the surface of CuNCs and CDs have been combined (He et al., 2018). In addition, the structure and composition of CDs/CuNCs were further explored using XPS spectra. As shown in Fig. 1(D), XPS spectrum of the synthesized CDs/CuNCs reveals the presence of S, C, O, N, Cu, and Na. It can be seen in the inset that characteristic peaks of Cu(0) 2p<sub>3/2</sub> and 2p<sub>1/2</sub> appear at 932.3 eV and

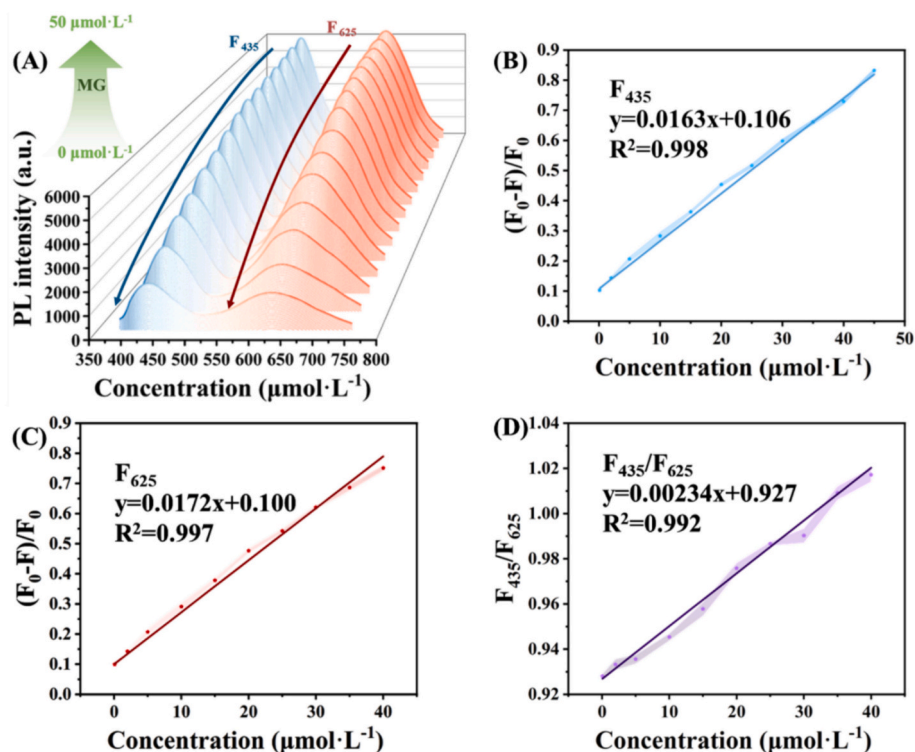


**Fig. 3.** (A) Fluorescence emission spectra of CDs/CuNCs with adding different concentrations of MG; (B) The linear relationship between  $[(F - F_0)/F_0]$  at 435 nm versus the concentration of MG from 0.1 to 45  $\mu\text{mol L}^{-1}$ ; (C) The linear relationship between  $[(F - F_0)/F_0]$  at 625 nm versus the concentration of MG from 0.1 to 40  $\mu\text{mol L}^{-1}$ ; (D) The relationship between the intensity ratio ( $F_{435}/F_{625}$ ) and the concentration of MG from 0.05 to 40  $\mu\text{mol L}^{-1}$ . Conditions: CDs/CuNCs, 1.5  $\text{mg mL}^{-1}$ ; BR buffer, pH 7.0; excitation, 376 nm.

953.2 eV, respectively, while no peak is observed at 942 eV, indicating that GSH successfully reduced copper from 2 to 0 valence (J. Q. Zhang, Pang, & Shen, 2023). To verify the primary binding force, the zeta potentials of CuNCs, CDs and CuNCs/CDs nanomaterials were tested. The CuNCs exhibited a zeta potential value of  $-16.41 \pm 1.13$  eV, which was attributed to the presence of carboxyl groups on their surface. In contrast, the CDs had a zeta potential value of  $+7.21 \pm 0.52$  eV, due to the abundance of amine groups exposed on their surface. When these two components were mixed, the resulting CuNCs/CDs probe exhibited a zeta potential value of  $-11.78 \pm 0.66$  eV. This observation suggests that there was charge-charge interactions between the CuNCs and CDs (Fig. S2).

### 3.3. Optical properties of CDs/CuNCs and its interaction with MG

We further explored the optical properties of the prepared CDs and CDs/CuNCs nanocomposite. As shown in Fig. 2(A), the UV-vis absorption spectra of CDs exhibits the absorption peaks at 232 and 320 nm, which could correspond to the  $\pi \rightarrow \pi^*$  and  $n \rightarrow \pi^*$  transitions, respectively (Hu, Gao, & Luo, 2021). When the excitation wavelength is 376 nm, the fluorescence emission wavelength is 438 nm. From Fig. 2(B), CDs/CuNCs nanocomposite exhibits excitation wavelength dependence. As the excitation wavelength changing from 336 to 436 nm, the fluorescence emission peak of CDs shows red shifts, while the peak position of CuNCs remains unchanged. To achieve the desired positions and intensities of the two peaks for application, the optimal excitation wavelength is 376 nm, resulting in corresponding emission wavelengths at 435 nm and 625 nm, with comparable intensities (Fig. 2(C)). UV-vis absorption spectrum illustrates that CDs/CuNCs have a broad absorption band from 290 to 337 nm. This molecular-like optical transition is due to the quasi-continuous electronic energy band structure and quantum confinement effects in both CDs and CuNCs. In addition, no signal of surface plasmon resonance of Cu nanoparticles appears near

560 nm, indicating that the size of the as-prepared CuNCs is smaller than 5 nm (Liu, Wang, Li, Rui, & Zeng, 2015).

### 3.4. Stability of the CDs/CuNCs

In order to further explore the application potential of CDs/CuNCs, we evaluated the stability of pH, salt concentration and storage time. The fluorescence properties of nanomaterials correlate closely with the pH of the analysis system. Fig. S3(A) demonstrates the fluorescence intensity of CDs/CuNCs (50  $\mu\text{L}$ , 1.5  $\text{mg mL}^{-1}$ ) in a series of BR buffer solutions ( $v = 2.0$  mL) with pH ranging from 2.0 to 12.0 to investigate the effect of pH on the intensity of both emission peaks of CDs/CuNCs ( $F_{435}$  and  $F_{625}$ ). Considering both peaks exhibited high intensity and stability within the pH range of 6.0–9.0, we chose pH 7.0 as the experimental condition to reduce potential interference factors. The salt concentration of the solution is also an important factor affecting the fluorescence intensity of nanomaterials. We examined the effect of varying salt concentration on the fluorescence intensity of CDs/CuNCs by adjusting the concentrations of NaCl. The results are presented in Fig. S3(B), showing that within the range of 0–1  $\text{mol L}^{-1}$ , the effect of ionic strength on fluorescence intensity was negligible. The stability of the fluoroprobe is one of the important parameters to evaluate its performance, and we examined the effect of storage time on the fluorescence intensity of CDs/CuNCs (Fig. S3(C)). Results show that the nanocomposite remained stable for 3 weeks, subsequently exhibiting a gradual decline.

### 3.5. Response and the reproducibility of CDs/CuNCs to MG concentration

The determination of MG by CDs/CuNCs was completed in BR buffer solution (pH = 7.0), the incubation time is 2 min (Fig. S4). The response of fluorescence signal of CDs/CuNCs to MG is shown in Fig. 3(A). Both signals of blue fluorescence at 435 nm and the red fluorescence at 625

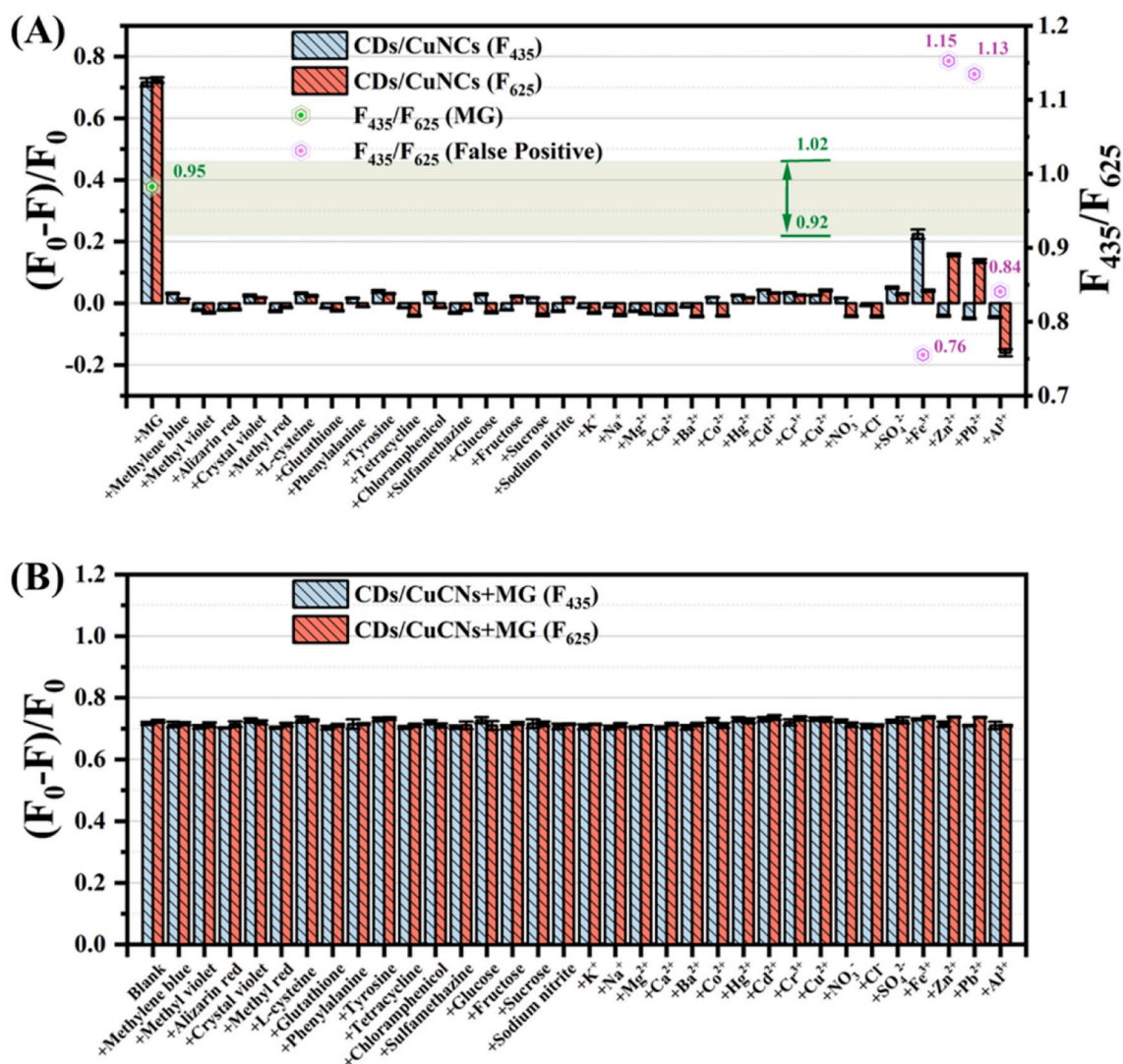


**Fig. 4.** (A) Selectivity evaluation. Relative emission intensity  $[(F_0 - F)/F_0]$  of as-prepared CDs/CuNCs after the addition of  $0.3 \text{ mmol L}^{-1}$  of different substances including organic dyes, antibiotics, food additives, anions and cations. After addition of these substances separately, fluorescence intensity ratio ( $F_{435}/F_{625}$ ) of CDs/CuNCs (0.92–1.02 is the range of variation in  $F_{435}/F_{625}$  within the linear range in Fig. 3(D), highlighted by the green region). (B) Anti-interference evaluation. The relative emission intensity  $[(F_0 - F)/F_0]$  of the as-prepared CDs/CuNCs (containing  $0.03 \text{ mmol L}^{-1}$  MG) was tested after the addition of  $0.3 \text{ mmol L}^{-1}$  of the fore-mentioned substances, excluding  $\text{Fe}^{3+}$ ,  $\text{Zn}^{2+}$ ,  $\text{Pb}^{2+}$ , and  $\text{Al}^{3+}$  (which were added at a concentration of  $0.09 \text{ mmol L}^{-1}$  each).  $F_0$  and  $F$  are the maximum emission intensities of the CDs/CuNCs before and after the addition of the substances. Conditions: CDs/CuNCs,  $1.5 \text{ mg mL}^{-1}$ ; BR buffer, pH 7.0; excitation, 376 nm. (For interpretation of the references to colour in this figure legend, the reader is referred to the web version of this article.)

nm decreased with the increase of MG concentration, simultaneously. The linear relationship between MG concentration and  $[(F_0 - F)/F_0]$ , which is related to  $F_{435}$  and  $F_{625}$  respectively, was obtained by fitting the curves shown in Fig. 3(B) and 3(C). Herein,  $F_0$  represents the fluorescence intensity in the absence of MG, while  $F$  represents the fluorescence intensity in the presence of MG. The linear regression equations are  $(F_0 - F)/F_0 = 0.013x + 0.126$  ( $R^2 = 0.998$ ) and  $(F_0 - F)/F_0 = 0.011x + 0.092$  ( $R^2 = 0.997$ ) ( $x$  is MG concentration,  $\mu\text{mol L}^{-1}$ ) with range of  $0.1\text{--}45 \mu\text{mol L}^{-1}$  and  $0.1\text{--}40 \mu\text{mol L}^{-1}$ , respectively. The corresponding LOD (limit of detection) are calculated to be  $62.54 \text{ nmol L}^{-1}$  and  $23.46 \text{ nmol L}^{-1}$  ( $S/N = 3$ ). The ratio  $F_{435}/F_{625}$  has a good linear correlation in the MG concentration range of  $0.05\text{--}40 \mu\text{mol L}^{-1}$ . The regression equation was  $F_{435}/F_{625} = 0.020x + 0.816$  ( $R^2 = 0.992$ ), and the LOD was calculated to be  $18.2 \text{ nmol L}^{-1}$  (Fig. 3(D)), and the limit of quantitation was  $60.73 \text{ nmol L}^{-1}$ . The results show that the ratio method has a higher sensitivity. To analyze the reproducibility of the preparation process of CDs/CuNCs fluorescent probe, six CDs/CuNCs were prepared according to the experimental procedure 2.3, and  $10.0 \mu\text{mol L}^{-1}$  MG was

measured separately. The results are shown in Table S1 with a relative standard deviation (RSD) of 3.95%. Furthermore, using the same CDs/CuNCs probe, we continuously measured MG 10 times, achieving a sensor response with an RSD of 3.16% (Table S2). The experimental results clearly indicate that the reproducibility of the sensor's fabrication and detection is acceptable. Compared with other MG detection methods (Table S3), the CDs/CuNCs used in this method has inexpensive raw materials and a simple synthesis process. The dual-signal ratio-metric fluorescence method incorporates built-in background interference correction, eliminating the influence of instrumental noise, light source intensity, probe concentration, and ambient environment, and thereby improving the signal-to-noise ratio. This method boasts a low LOD, high recovery rates, and good reproducibility. Its advantages in selectivity and anti-interference will be further discussed in Section 3.6.

### 3.6. Selectivity and anti-interference

To evaluate the selectivity and anti-interference of CDs/CuNCs, we

**Table 1**The results of detect method ( $n = 6$ ) in different fish sample.

Sample	This method				HPLC		
	Spiked ( $\mu\text{mol L}^{-1}$ )	Found ( $\mu\text{mol L}^{-1}$ )	Recovery (%)	RSD (%)	Found ( $\mu\text{mol L}^{-1}$ )	Recovery (%)	RSD (%)
Silver carp	0	ND			ND		
	1.0	1.02	102.0	2.9	0.96	96.0	3.6
	5.0	5.17	103.4	3.0	5.11	102.2	2.9
	10.0	9.96	99.6	2.6	10.16	101.6	3.9
	15.0	14.74	98.3	3.2	15.48	103.2	3.0
Carp	0	ND			ND		
	1.0	0.97	97.0	3.1	1.02	102.0	3.3
	5.0	4.98	99.6	2.8	5.17	103.4	3.8
	10.0	10.32	103.2	3.3	10.26	102.6	2.8
	15.0	15.24	101.6	3.1	15.57	103.8	3.2

ND: Not detected.

introduced different potential coexisting substances into the analytical system. These substances included antibiotics commonly used in aquaculture like tetracycline, chloramphenicol, and sulfamethazine; as well as amino acids, such as L-cysteine, glutathione, phenylalanine, and tyrosine. Moreover, we incorporated organic dyes that are potentially present in industrial sewage, including methylene blue, methyl violet, alizarin red, crystal violet, and methyl red. Sugar additives like glucose, fructose, and sucrose, which are widely used in food processing, were also included. Furthermore, we tested heavy metal ions prone to bioaccumulation, such as  $\text{Hg}^{2+}$ ,  $\text{Cd}^{2+}$ ,  $\text{Cr}^{3+}$ ,  $\text{Cu}^{2+}$ , and  $\text{Pb}^{2+}$ . Finally, we considered common anions and cations typically present in environmental sewage, including  $\text{K}^+$ ,  $\text{Na}^+$ ,  $\text{Mg}^{2+}$ ,  $\text{Ca}^{2+}$ ,  $\text{Ba}^{2+}$ ,  $\text{Co}^{2+}$ ,  $\text{Fe}^{3+}$ ,  $\text{Zn}^{2+}$ ,  $\text{Al}^{3+}$ ,  $\text{NO}_3^-$ ,  $\text{Cl}^-$ , and  $\text{SO}_4^{2-}$ .

In Fig. 4(A), most of the fore-mentioned substances have no significant influence on both  $F_{435}$  and  $F_{625}$  of the system. However, the presence of  $\text{Fe}^{3+}$  quenched  $F_{435}$ , resulting in an  $F_{435}/F_{625}$  ratio (represented as R) of 0.76. On the other hand, the presence of  $\text{Pb}^{2+}$  and  $\text{Zn}^{2+}$  lead to the quenching of  $F_{625}$  ( $R = 1.15$  and  $1.34$ ). Conversely, the presence of  $\text{Al}^{3+}$  had an enhancing effect on  $F_{625}$  ( $R = 0.84$ ). So, using only  $F_{435}$  or  $F_{625}$  to determine MG would cause false positives. To avoid this situation, the dual-signal response strategy was used. When the analyte is MG, the detection results of the two signals should be consistent. Furthermore, as the two signals exhibit a similar trend of change, the ratio R varies within a specific range, from  $R_{\text{bottom}}$  to  $R_{\text{top}}$ . In this study, R belongs to the range of 0.92–1.02, which corresponds to the range of  $F_{435}/F_{625}$  in Fig. 3(D). Since the R values of systems containing  $\text{Fe}^{3+}$ ,  $\text{Pb}^{2+}$ ,  $\text{Zn}^{2+}$ , and  $\text{Al}^{3+}$  did not fall within the established range, it indicates that it was not MG that affected the fluorescence signal of the system, thus demonstrating the high specificity of the method.

Then, we investigated the interference of the above substances on the system at MG concentration  $0.03 \text{ mmol L}^{-1}$ . The Fig. 4(B) show that the majority of potential interfering substances, at concentrations below  $0.3 \text{ mmol L}^{-1}$ , and  $\text{Fe}^{3+}$ ,  $\text{Pb}^{2+}$ ,  $\text{Zn}^{2+}$ , and  $\text{Al}^{3+}$  at concentrations below  $0.09 \text{ mmol L}^{-1}$ , have minimal effects on  $F_{435}$  and  $F_{625}$ . Accordingly, the ability of the fluoroprobe CDs/CuNCs for MG specific detection was verified.

### 3.7. Possible detection mechanism

Generally, the fluorescence quenching mechanisms of CDs and CuNCs can be attributed to static quenching effect (SQE), dynamic quenching effect (DQE), Förster resonance energy transfer (FRET), and IFE. The quenching mechanisms were studied through fluorescence lifetime decay curves, UV–visible spectra, and fluorescence spectra.

Firstly, by fitting the data, the fluorescence lifetimes of CDs/CuNCs were determined to be  $5.46 \text{ ns}$  without MG and  $5.51 \text{ ns}$  with MG (Fig. S5 (A)). The minimal change in fluorescence lifetime indicated that SQE or IFE are the dominant factors, while DQE and FRET can be excluded. SQE implies that the fluorescent material may react with a receptor to form a non-fluorescent complex, which can be observed in the UV–visible

absorption spectrum. As can be seen from the Fig. S5(B), no new peak appeared after adding MG, indicating that SQE is ruled out. IFE is caused by the overlap between the UV–visible absorption spectrum of the receptor and the fluorescence emission spectrum of the probe. Referring to Fig. 2(D), the absorption spectrum of MG shows two peaks at 424 and 618 nm, which overlap with the two emission peaks of CDs/CuNCs located at 435 and 625 nm, respectively. Furthermore, the simultaneous quenching of the fluorescence peaks of the CDs/CuNCs suggests that the mechanism may be IFE, aligning with our design strategy.

### 3.8. Application of CDs/CuNCs sensor in real fish samples

To assess the accuracy of the ratiometric fluorescence method in practical applications, we made a comparison with the HPLC method for the detection of MG in fish samples. The chromatographs and correlation curve shown in Fig. S6. The samples with MG concentration of 1.0, 5.0, 10.0, 15.0  $\mu\text{mol L}^{-1}$  were tested, and each concentration were measured six time. The results of the proposed method were in agreement with the HPLC method with recoveries ranging from 96.0% to 103.8% and RSD was  $<3.3\%$ . (shown in Table 1).

## 4. Conclusion

In summary, we developed a highly selective dual-signal response ratiometric fluorescence sensing method for MG detection based on CDs/CuNCs nanocomposite. The method has been successfully applied to trace the amount of MG in the fish samples with the recovery over 96%. The simple, rapid and reliable dual response signals ratiometric fluorescence sensing strategy opens up attractive perspectives for MG detection. It shows great potential in food, environmental and bio-analytical applications.

### CRediT authorship contribution statement

**Jun-Qiu Zhang:** Writing – original draft, Methodology, Investigation, Formal analysis, Data curation, Conceptualization. **Xiao-Fang Shen:** Writing – review & editing, Resources, Project administration, Funding acquisition, Conceptualization. **Jun Liu:** Project administration, Funding acquisition.

### Declaration of competing interest

The authors declare that they have no known competing financial interests or personal relationships that could have appeared to influence the work reported in this paper.

### Data availability

Data will be made available on request.

## Acknowledgements

This work was supported by the Science and Technology Innovation Talent Program of Sichuan Province of China (2023JDR0007), the National Key Research and Development Program of China (2022YFF1100803).

## Appendix A. Supplementary data

Supplementary data to this article can be found online at <https://doi.org/10.1016/j.foodchem.2024.139543>.

## References

- Andersen, W. C., Turnipseed, S. B., Karbiwnyk, C. M., Lee, R. H., Clark, S. B., Rowe, W. D., & Miller, K. E. (2009). Multiresidue method for the triphenylmethane dyes in fish: Malachite green, crystal (gentian) violet, and brilliant green. *Analytica Chimica Acta*, 637(1–2), 279–289. <https://doi.org/10.1016/j.aca.2008.09.041>
- Bai, H. Y., Tu, Z. Q., Liu, Y. T., Tai, Q. X., Guo, Z. K., & Liu, S. Y. (2020). Dual-emission carbon dots-stabilized copper nanoclusters for ratiometric and visual detection of  $\text{Cr}_2\text{O}_7^{2-}$  ions and  $\text{Cd}^{2+}$  ions. *Journal of Hazardous Materials*, 386. <https://doi.org/10.1016/j.jhazmat.2019.121654>
- Chen, M., Huang, Y. Q., Miao, J. J., Fan, Y. X., & Lai, K. Q. (2023). A highly sensitive surface-enhanced Raman scattering sensor with MIL-100 (Fe)/Au composites for detection of malachite green in fish pond water. *Spectrochimica Acta Part a-Molecular and Biomolecular Spectroscopy*, 292. <https://doi.org/10.1016/j.saa.2023.122432>
- Cheng, S. J., Wang, X., Yan, X. R., Xiao, Y. T., & Zhang, Y. (2022). Simple synthesis of green luminescent N-doped carbon dots for malachite green determination. *Analytical Methods*, 14(26), 2616–2622. <https://doi.org/10.1039/d2ay00682k>
- Culp, S. J., & Beland, F. A. (1996). Malachite green: A toxicological review. *Journal of the American College of Toxicology*, 15(3), 219–238. <https://doi.org/10.3109/10915819609008715>
- Culp, S. J., Blankenship, L. R., Kusewitt, D. F., Doerge, D. R., Mulligan, L. T., & Beland, F. A. (1999). Toxicity and metabolism of malachite green and leucomalachite green during short-term feeding to Fischer 344 rats and B6C3F<sub>1</sub> mice. *Chemico-Biological Interactions*, 122(3), 153–170. [https://doi.org/10.1016/s0009-2797\(99\)00119-2](https://doi.org/10.1016/s0009-2797(99)00119-2)
- Esmail, L. A., & Jabbar, H. S. (2023). Violuric acid carbon dots as a highly fluorescence probe for ultrasensitive determination of Zn (II) in tomato paste. *Food Chemistry*, 413. <https://doi.org/10.1016/j.foodchem.2023.135638>
- Gao, Z. X., Li, Y. Y., Ma, Y. L., Ji, W. X., Chen, T., Ma, X. X., & Xu, H. (2019). Functionalized melamine sponge based on  $\beta$ -cyclodextrin-graphene oxide as solid-phase extraction material for rapidly pre-enrichment of malachite green in seafood. *Microchemical Journal*, 150. <https://doi.org/10.1016/j.microc.2019.104167>
- He, Q. G., Wang, B., Liang, J., Liu, J., Liang, B., Li, G. L., & Liu, H. M. (2023). Research on the construction of portable electrochemical sensors for environmental. *Materials Today Advances*, 17. <https://doi.org/10.1016/j.mtadv.2022.100340>
- He, W. J., Gui, R. J., Jin, H., Wang, B. Q., Bu, X. N., & Fu, Y. X. (2018). Ratiometric fluorescence and visual imaging detection of dopamine based on carbon dots/copper nanoclusters dual-emitting nanohybrids. *Talanta*, 178, 109–115. <https://doi.org/10.1016/j.talanta.2017.09.019>
- Hu, Y., Gao, Z., & Luo, J. (2021). Fluorescence detection of malachite green in fish tissue using red emissive Se,N,Cl-doped carbon dots. *Food Chemistry*, 335. <https://doi.org/10.1016/j.foodchem.2020.127677>
- Jiang, Y. W., Sima, Y., Liu, L., Zhou, C. Q., Shi, S. T., Wan, K., & Liu, J. (2024). Research progress on portable electrochemical sensors for detection of mycotoxins in food and environmental samples. *Chemical Engineering Journal*, 485. <https://doi.org/10.1016/j.cej.2024.149860>
- Khan, M., & Lively, J. A. (2020). Determination of sulfite and antimicrobial residue in imported shrimp to the USA. *Aquaculture Reports*, 18. <https://doi.org/10.1016/j.aqrep.2020.100529>
- Kong, Y. J., Hou, G. Z., Gong, Z. N., Zhao, F. T., & Han, L. J. (2022). Fluorescence detection of malachite green and cations ( $\text{Cr}^{3+}$ ,  $\text{Fe}^{3+}$  and  $\text{Cu}^{2+}$ ) by a europium-based coordination polymer. *RSC Advances*, 12(14), 8435–8442. <https://doi.org/10.1039/d2ra00077f>
- Kraai, J. A., Rorrer, G. L., & Wang, A. X. (2019). Highly-porous diatom biosilica stationary phase for thin-layer chromatography. *Journal of Chromatography A*, 1591, 162–170. <https://doi.org/10.1016/j.chroma.2019.01.037>
- Li, N. L., Li, R. H., Song, Y. S., Ma, L., Gao, C. L., Li, L. L., & Zhan, J. H. (2020). Caramelized carbonaceous shell-coated  $\gamma\text{-Fe}_2\text{O}_3$  as a magnetic solid-phase extraction sorbent for LC-MS/MS analysis of triphenylmethane dyes. *Microchimica Acta*, 187(7). <https://doi.org/10.1007/s00604-020-04346-z>
- Li, W. T., Hu, X. T., Li, Q., Shi, Y. Q., Zhai, X. D., Xu, Y. W., & Kang, S. F. (2020). Copper nanoclusters @ nitrogen-doped carbon quantum dots-based ratiometric fluorescence probe for lead (II) ions detection in porphyrin. *Food Chemistry*, 320. <https://doi.org/10.1016/j.foodchem.2020.126623>
- Li, Z. L., Pang, S. J., Wang, M., Wu, M., Li, P. J., Bai, J. N., & Yang, X. D. (2021). Dual-emission carbon dots-copper nanoclusters ratiometric photoluminescent nanocomposites for highly sensitive and selective detection of  $\text{Hg}^{2+}$ . *Ceramics International*, 47(13), 18238–18245. <https://doi.org/10.1016/j.ceramint.2021.03.143>
- Li, Z. Y., Shen, T., Gu, J. X., & Chattha, S. A. (2022). PVP-gold-copper nanocluster based NIR fluorescence probe for sensitive detection of malachite green. *New Journal of Chemistry*, 46(4), 1658–1664. <https://doi.org/10.1039/d1nj04943g>
- Liu, P., Wang, H., Li, X., Rui, M., & Zeng, H. (2015). Localized surface plasmon resonance of Cu nanoparticles by laser ablation liquid media. *RSC Advances*, 5(97), 79738–79745. <https://doi.org/10.1039/c5ra14933a>
- Luo, X. W., Chen, Z. F., Li, H. F., Li, W. Q., Cui, L., & Huang, J. H. (2019). Exploiting the application of l-aptamer with excellent stability: An efficient sensing platform for malachite green in fish samples. *Analyst*, 144(14), 4204–4209. <https://doi.org/10.1039/c9an00332k>
- Luo, Y. Z., & Li, Z. Y. (2022). A sensitive electrochemical sensor manufactured from multi-wall carbon nanotubes-polyethylenimine nanocomposite for malachite green detection. *Journal of Alloys and Compounds*, 897, 4204–4209. <https://doi.org/10.1016/j.jallcom.2021.163216>
- Magesa, F., Wu, Y. Y., Tian, Y. L., Vianney, J. M., Buza, J., He, Q. G., & Tan, Y. M. (2019). Graphene and graphene like 2D graphitic carbon nitride: Electrochemical detection of food colorants and toxic substances in environment. *Trends in Environmental Analytical Chemistry*, 23. <https://doi.org/10.1016/j.teac.2019.e00064>
- Pei, X. Y., Pan, Y., Zhang, L. C., & Lv, Y. (2021). Recent advances in ratiometric luminescence sensors. *Applied Spectroscopy Reviews*, 56(4), 1386–1425. <https://doi.org/10.1016/j.saa.2023.122697>
- Qiu, J. Y., Na, L. H., Li, Y. M., Bai, W. F., Zhang, J. P., & Jin, L. (2022). N,S-GQDs mixed with CdTe quantum dots for ratiometric fluorescence visual detection and quantitative analysis of malachite green in fish. *Food Chemistry*, 390. <https://doi.org/10.1016/j.foodchem.2022.133156>
- Qu, S. N., Chen, H., Zheng, X. M., Cao, J. S., & Liu, X. Y. (2013). Ratiometric fluorescent nanosensor based on water soluble carbon nanodots with multiple sensing capacities. *Nanoscale*, 5(12), 5514–5518. <https://doi.org/10.1039/c3nr00619k>
- Sacara, A. M., Cristea, C., & Muresan, L. M. (2017). Electrochemical detection of malachite green using glassy carbon electrodes modified with CeO<sub>2</sub> nanoparticles and Nafion. *Journal of Electroanalytical Chemistry*, 792, 23–30. <https://doi.org/10.1016/j.jelechem.2017.03.030>
- Samiey, B., & Toosi, A. R. (2010). Adsorption of malachite green on silica gel: Effects of NaCl, pH and 2-propanol. *Journal of Hazardous Materials*, 184(1–3), 739–745. <https://doi.org/10.1016/j.jhazmat.2010.08.101>
- Sanjay, B. P., Sandeep, S., Santhosh, A. S., Karthik, C. S., Varun, D. N., Swamy, N. K., & Muthusamy, K. (2022). Unprecedented 2D GNR-CoB nanocomposite for detection and degradation of malachite green - A computational prediction of degradation pathway and toxicity. *Chemosphere*, 287. <https://doi.org/10.1016/j.chemosphere.2021.132153>
- Sharma, P., Naithani, S., Layek, S., Kumar, A., Rawat, R., Heena, Kaja, S., Nag, A., Kumar, S., & Goswami, T. (2023). Development of low-cost copper nanoclusters for highly selective "turn-on" sensing of Hg<sup>2+</sup> ions. *Spectrochimica Acta Part a-Molecular and Biomolecular Spectroscopy*, 297, 206–211. <https://doi.org/10.1016/j.saa.2015.08.004>
- Shen, Y. D., Deng, X. F., Xu, Z. L., Wang, Y., Lei, H. T., Wang, H., & Sun, Y. M. (2011). Simultaneous determination of malachite green, brilliant green and crystal violet in grass carp tissues by a broad-specificity indirect competitive enzyme-linked immunosorbent assay. *Analytica Chimica Acta*, 707(1), 148–154. <https://doi.org/10.1016/j.aca.2011.09.006>
- Simoes, E. F. C., Leitao, J. M. M., & da Silva, J. (2016). Carbon dots prepared from citric acid and urea as fluorescent probes for hypochlorite and peroxyxynitrite. *Microchimica Acta*, 183(5), 1769–1777. <https://doi.org/10.1007/s00604-016-1807-6>
- Srivastava, S., Sinha, R., & Roy, D. (2004). Toxicological effects of malachite green. *Aquatic Toxicology*, 66(3), 319–329. <https://doi.org/10.1016/j.aquatox.2003.09.008>
- Wan, H. P., Weng, S. P., Liang, L. Z., Lu, Q. H., & He, J. G. (2011). Evaluation of the developmental toxicity of leucomalachite green administered orally to rats. *Food and Chemical Toxicology*, 49(12), 3031–3037. <https://doi.org/10.1016/j.fct.2011.10.003>
- Wang, F., Wang, H., Shen, Y. D., Li, Y. J., Dong, J. X., Xu, Z. L., & Xiao, Z. L. (2016). Bispecific monoclonal antibody-based Multianalyte ELISA for Furalatadone metabolite, malachite green, and Leucomalachite green in aquatic products. *Journal of Agricultural and Food Chemistry*, 64(42), 8054–8061. <https://doi.org/10.1021/acs.jafc.6b03233>
- Yan, Y. H., Sun, J., Zhang, K., Zhu, H. J., Yu, H., Sun, M. T., & Wang, S. H. (2015). Visualizing gaseous nitrogen dioxide by Ratiometric fluorescence of carbon Nanodots-quantum dots hybrid. *Analytical Chemistry*, 87(4), 2087–2093. <https://doi.org/10.1021/ac503474x>
- Yu, S. L., Yuan, X. J., Yang, J., Yuan, J. T., Shi, J. H., Wang, Y. L., & Gao, S. F. (2015). A chemometric-assisted method for the simultaneous determination of malachite green and crystal violet in water based on absorbance-pH data generated by a homemade pH gradient apparatus. *Spectrochimica Acta Part a-Molecular and Biomolecular Spectroscopy*, 150, 403–408. <https://doi.org/10.1016/j.saa.2015.05.060>
- Yue, X. Y., Fu, L., Li, Y., Xu, S., Lin, X., & Bai, Y. H. (2023). Lanthanide bimetallic MOF-based fluorescent sensor for sensitive and visual detection of sulfamerazine and malachite. *Food Chemistry*, 410. <https://doi.org/10.1016/j.foodchem.2023.135390>
- Zhang, J. Q., Pang, Y. H., & Shen, X. F. (2023). Rapid microwave-assisted synthesis of copper nanoclusters for "on-off-on" fluorescent sensor of tert-butylhydroquinone in edible oil. *Microchemical Journal*, 193. <https://doi.org/10.1016/j.microc.2023.109070>
- Zhang, Y. Y., Xu, H. D., Yang, Y. L., Zhu, F. M., Pu, Y. X., You, X. S., & Liao, X. L. (2021). Efficient fluorescence resonance energy transfer-based ratiometric fluorescent probe for detection of dopamine using a dual-emission carbon dot-gold nanocluster

- nanohybrid. *Journal of Photochemistry and Photobiology a-Chemistry*, 411. <https://doi.org/10.1016/j.jphotochem.2021.113195>
- Zhou, J. F., Zhou, Q., & Chu, C. J. (2022). Dyes-modified metal-organic frameworks composite as a sensitive, reversible and ratiometric fluorescent probe for the rapid detection of malachite green. *Microchemical Journal*, 180. <https://doi.org/10.1016/j.microc.2022.107631>
- Zhu, S. J., Meng, Q. N., Wang, L., Zhang, J. H., Song, Y. B., Jin, H., & Yang, B. (2013). Highly Photoluminescent carbon dots for multicolor patterning, sensors, and bioimaging. *Angewandte Chemie, International Edition*, 52(14), 3953–3957. <https://doi.org/10.1002/anie.201300519>